8 Jun 87 Conference Presentation

Comparisons of Unsteady Flow Fields about Straight and Swept Wings Using Flow Visualization and Hotwire Anemometry

TA 2307-F1-38

J. Ashworth, S. Huyer, M. Luttges

F.J. Seiler Research Laboratory
USAF Academy CO 80840-6528

FJSRL-PR-90-0012

The three-dimensional, spatial and temporal unsteady flow characteristics induced by dynamic sinusoidal oscillations of different sweep geometry finite wings were investigated. The span-dependent, finite wing flow interactions between unsteady wingtip and leading edge vortical structures were documented for three sweep configurations (30 deg forward, zero, and 30 deg aft) using flow visualization and hotwire anemometry techniques. The three-dimensional flow field about the wings was investigated by recording flow visualization and hotwire data at numerous span locations from wingtip to wingroot. Hotwire velocity data was collected across the chordlength of each wing from leading to trailing edge. The hotwire data confirmed hypotheses formulated during flow visualization analyses and added quantifying magnitude information., All data recorded during these tests illustrated highly repeatable unsteady flow patterns which indicate promising beneficial aerodynamic flow characteristics when compared to static test at identical geometries.

hot wire anemometers 13
three dimensional flow
aerodynamic characteristics.

UNCLASSIFIED UNCLASSIFIED UNCLASSIFIED NONE

AIAA'87

AIAA-87-1334
Comparisons of Unsteady Flow Fields about Straight and Swept Wings Using Flow Visualization and Hotwire Anemometry

J. Ashworth, S. Huyer and M. Luttges
University of Colorado, Boulder, CO

AIAA 19th Fluid Dynamics, Plasma Dynamics and Lasers Conference
June 8-10, 1987/Honolulu, Hawaii

COMPARISONS OF UNSTEADY FLOW FIELDS ABOUT STRAIGHT AND SWEPT WINGS USING FLOW VISUALIZATION AND HOTWIRE ANEMOMETRY

J. Ashworth*, S. Huyer** and M. Luttges***
Aerospace Engineering Sciences
University of Colorado, Campus Box 429
Boulder, Colorado 80309

Abstract

The three-dimensional, spatial and temporal unsteady flow characteristics induced by dynamic sinusoidal oscillations of different sweep geometry finite wings were investigated. The span-dependent, finite wing flow interactions between unsteady wingtip and leading edge vortical structures were documented for three sweep configurations (30° forward, 0° and 30° aft) using flow visualization and hotwire anemometry techniques. The three-dimensional flow field about the wings was investigated by recording flow visualization and hotwire data at numerous span locations from wingtip to wingroot. Hotwire velocity data was collected across the chordlength of each wing from leading to trailing edge. The hotwire data confirmed hypotheses formulated during flow visualization analyses and added quantifying magnitude information. All data recorded during these tests illustrated highly repeatable unsteady flow patterns which indicate promising beneficial aerodynamic flow characteristics when compared to static tests at identical geometric conditions.

*Major, USAF
Associate Professor, Department of Aeronautics, U. S. Air Force Academy, Colorado Springs, CO
Member AIAA

**Graduate Research Assistant, Department of Aerospace Engineering Sciences, University of Colorado, Boulder, CO
Member AIAA

***Professor, Department of Aerospace Engineering Sciences, University of Colorado, Boulder, CO
Member AIAA

Nomenclature

ASW	Aft swept wing
c	wing chordlength measured parallel to the freestream
C	Nondimensional chord position measured from wing leading edge
FSW	Forward swept wing
K	Nondimensional reduced frequency parameter, $K = \omega c/2 V_\infty$
S	Nondimensional spanwise distance from wingtip
STW	Straight wing
V	Local absolute velocity measured at hot wire probe position
V_∞	Freestream tunnel velocity
α	Instantaneous geometric angle of attack (degrees)
α_m	Mean angle of attack (degrees)
α_ω	Oscillation amplitude (degrees)
Λ	Wing sweep angle (30° forward or aft)
ϕ	Nondimensional oscillation phase angle (% cycle beginning at α_{max})
ω	Rotational frequency in radians per second

Introduction

High performance aircraft must utilize swept wing technology to be efficient at high airspeeds[1,2]. Both recent aerodynamic technology and modern computer actuated control surfaces of these aircraft currently allow maximum performance during mid and high airspeed flight. The utilization of forced unsteady flows by these swept wing configurations seems increasingly more feasible and may be employed to expand flight envelopes in the low speed regime. Effective application using such flows can be realized only after extensive evaluations of the three-dimensional dynamic stall regions produced about swept wing configurations as well as a variety of body shapes.

Previous experimental investigations of unsteady flow fields about two-dimensional airfoils[3-9], three-dimensional straight and swept wings[10-17], wings subjected to accelerating flows[18] and

wings in high angle of attack pitching motions[19,20] show that transient lift enhancement is generated by forced unsteady flows. The effects of three-dimensional unsteady motion on the flows produced about swept wings have been visualized but the magnitudes of these flows remain unclear. This study focuses on a comparison between visualized flow fields and hotwire velocity measurements.

Methods

Initial geometric comparison studies between the forward swept wing (FSW), straight wing (STW) and aft swept wing (ASW) were conducted in the 40.5 X 40.5 cm test section, low speed wind tunnel at the University of Colorado. The test section side wall and top are constructed of cast acrylic Plexiglas such that flow could be visualized from orthogonal perspectives. Walls not used for specific visualizations were painted flat black to help reduce light reflections during flow visualization tests. The tunnel freestream velocity was set to maintain a Reynolds number of 40,000.

A hollow core aluminum NACA 0015 airfoil section with 15.2 cm chordlength was used to manufacture the three wings. The wings were constructed with the quarterchord lines swept at three different sweep angles: 30° forward, 0°, and 30° aft. The root and tip of each wing were cut parallel to the angle of the oncoming flow and the wingtip cut was sealed with a flat plate fashioned to match the contour of the airfoil profile. With the sweep modifications, the effective chordlength for the FSW and ASW was 17.6 cm. The wings were mounted horizontally in the wind tunnel and were painted black to reduce reflection and permit flow structure visualizations very close to the surface.

An externally mounted, D.C. motor (1/6 h.p.) and scotch yoke mechanism produced sinusoidal pitching motion of variable amplitude and speed. The induced wing pitching motion was constant throughout the full length of the wing along an axis running through the quarterchord location. By adjusting the position of the shaft and scotch yoke, the mean angle and oscillation amplitude could be varied. A magnetic reed switch recorded the rotational frequency and triggered an electronic variable delay which allowed data recording at any desired position in the oscillation cycle. During the dynamic tests, the motion histories began at maximum α where $\phi = 0.0$, and returned to the highest α where $\phi = 1.0$.

Initial data were collected on the three wings using a flow visualization technique[17] which includes a smoke wire and stroboscopic photography to record the flow patterns. The wire could be positioned to cause the vertical smoke sheet to impinge on the wing surface at any desired span location. The multiple exposure photographs provided evidence of reliability in the observed flow field structures. To gain an orthogonal perspective, photographs were taken from the side, viewing along the wing span from tip to root, and from the top of the wind tunnel test section, viewing the top surface of the wing. In all the presented photographic visualizations, the flow is passing from left to right.

To make comprehensive comparisons of sweep angle effects, static conditions over all three wings were first evaluated across the α range of 3° to 27°. The dynamic tests of the three wings were accomplished using an α_m of 15° and an α_ω of ±10°. The reduced frequency values were varied from 0.6 to 1.4K. Photographs were prepared for discrete span locations, S, varying from the wingtip, 0.17c, 0.33c, 0.5c, 0.67c, 1.0c to 1.33c inboard. The entire sinusoidal oscillation period was examined by flow visualization, however, the photographic documentation reported here is only for those periods in the wing motion that were essential to understanding unsteady flow structure initiation and development. Vortex initiation point, vortex size, spatial time-dependent positions, shear layer development and boundary layer growth were quantified from the visualizations.

To quantify flow characteristics about the three wings, hotwire anemometry was used to record local velocity magnitudes. Measurements were obtained with a constant temperature hotwire probe constructed of 10% Rh Pt 0.0001 inch Wollaston wire. The linearized circuit, 0 to 5 volt full scale output, was preset for maximum anticipated velocity. Data acquisition and reduction were accomplished with a 16 channel DT 1761 Data Translation A/D interface (2 KHz) and Digital Equipment Corporation LSI 11/23 microprocessor. Data were reduced and then plotted on an Esterline Angus Model 575 x-y plotter.

To match the flow visualization data for the three wings, identical test conditions of Reynolds number, K value, spanwise location, α_m and α_ω were used. The anemometric measurements were taken at each span location and chordwise at 0.00c (leading edge), 0.17c, 0.33c, 0.50c, 0.67c, 0.83c and 1.00c. Phase-locked velocity sampling was done for ten runs (over 200 points per run) consisting of two complete oscillation cycles. Velocity magnitudes were taken simultaneously with orthogonal top and side view flow visualizations yielding flow direction. Wing motion prevented probe locations near the surface thus comprehensive velocity measurements of small vortical structures very near the wing surface were not possible.

Results

The three-dimensional unsteady flow fields produced by sinusoidal oscillation of these three wing configurations have been documented by flow visualization[17]. Spatial and temporal trends in the development of wingtip and leading edge vortices were characterized throughout the oscillation cycle. These tests illustrated a decrease in apparent size of the leading edge vortex and in the convective path length as flow fields were visualized proximal to the wingtip. The initiation position and magnitude of leading edge vortices were very dependent on wing sweep angle. The oscillating FSW produced leading edge vortices that continually increased in size and convective path length as distance from the wingtip increased. The unsteady flow about the STW shows comparatively more cohesive leading edge vortices which exhibit similar spanwise formation and convective tendencies inboard of a position 0.5c from the wingtip. The ASW initiates comparatively even larger leading edge structures with airfoil-like convective path lengths even very near the wingtip. A shear layer is formed under certain dynamic conditions on the surface of each wing at differing spanwise regions. The leading edge vortex sometimes, predominately on the FSW near the wingtip and the ASW near the wingroot, dissipates into this shear layer.

Flow visualization techniques provide documentation of fundamental unsteady flow characteristics elicited by the three geometrically distinct wings. Quantification and comparison of flow characteristics such as vortex size, position, temporal development, and convective tendencies can be achieved visually. Further quantification of the three-dimensional unsteady flow field about these wings must involve other data collection techniques. To strengthen or reject hypotheses arising from flow visualization studies, velocity data were used. Absolute velocities were recorded at spanwise locations previously visualized throughout the cyclic motion histories of the three wings. Chordwise and spanwise effects of wing sweep angle for identical test conditions (Re, K, α_m and α_ω) are recorded by visualization and anemometry techniques.

Flow visualization versus velocity comparisons are shown in Figs. 1 and 2 for the STW at K = 1.0 and S = 0.67c. The hotwire probe positions from leading edge (A) to trailing edge (G) can be seen in the left column of Fig. 1 for ϕ = 0.2 in the oscillation cycle. The right column contains spatially matched probe position velocity measurements computer plotted over two complete oscillation cycles. The ϕ = 0.2 point of each cycle is marked with dashed lines and are plotted for clarity in Fig. 2. The velocity

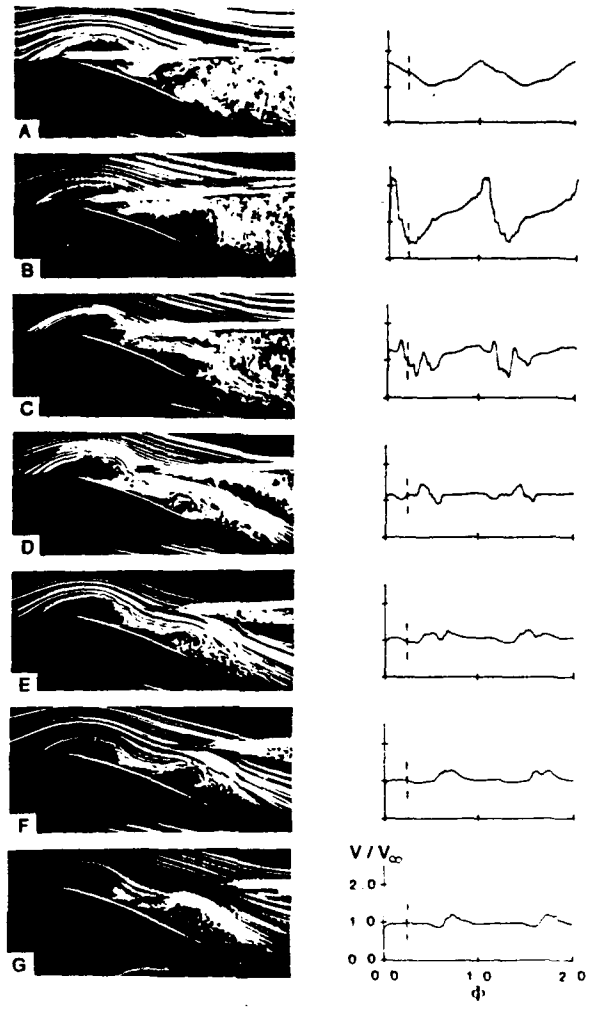

Fig. 1 Chordwise hotwire probe position and velocity data, STW, K = 1.0, S = 0.67c, A - G correspond to probe position and data at C= 0.00c, 0.17c, 0.33c, 0.50c, 0.67c, 0.83c and 1.00c.

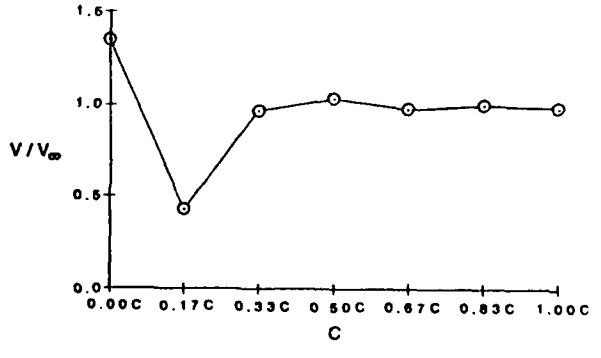

Fig. 2 Velocity comparison along chord-length, STW, K = 1.0, S = 0.67c, ϕ = 0.2.

comparisons at ϕ = 0.2 illustrate the unsteady fluid dynamic variations across the chord of the wing. The probe at the leading edge, Fig. 1 A, is positioned in

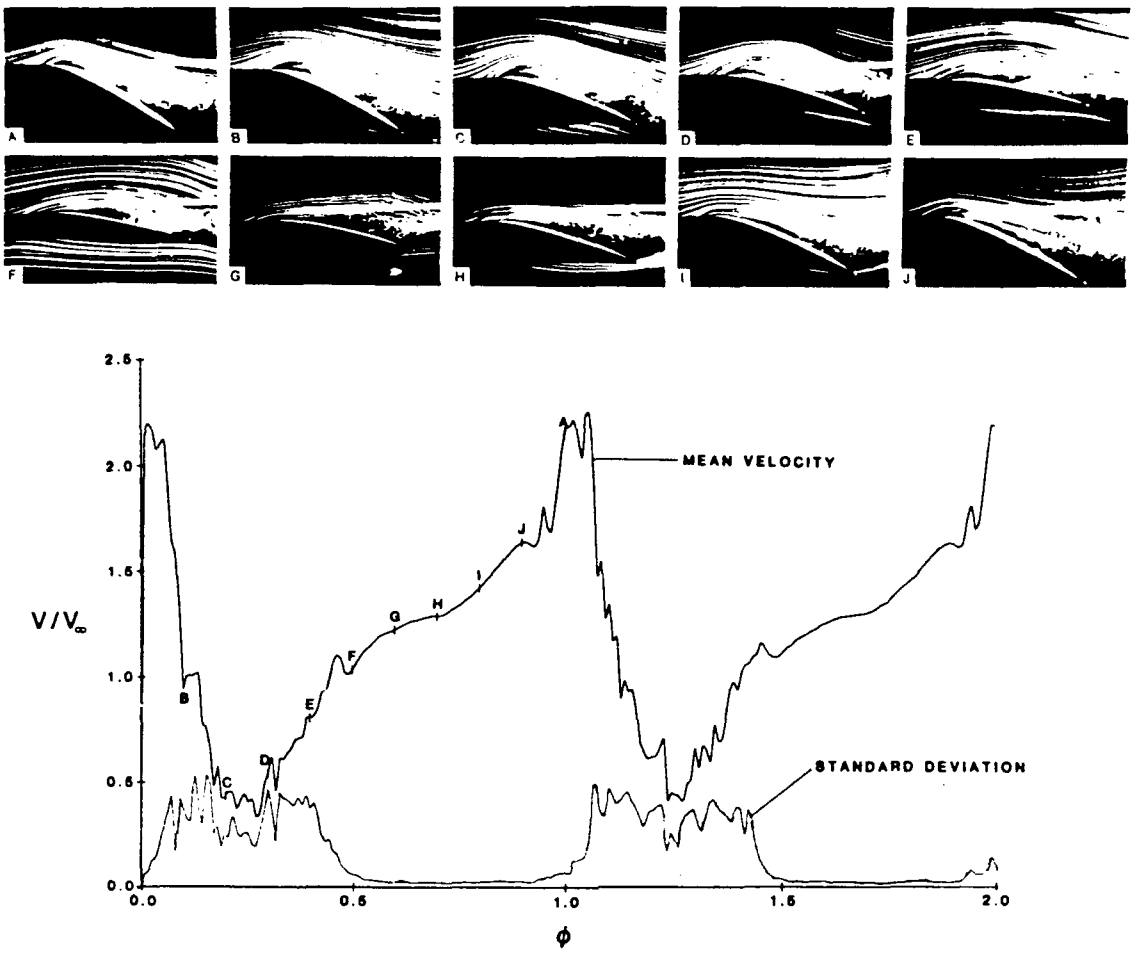

Fig. 3 Flow visualization and hotwire comparison, STW, K = 1.0, C = 0.17c, S = 0.67c.

the high velocity region of potential flow passing over the leading edge of the wing. Here at ϕ = 0.2 the local velocity is nearly 1.5 V_∞. At C = 0.17c, Fig. 1 B, the probe records the much lower velocity of the apparent interior of the dynamic stall vortex. When the probe is near the aft circumference of the vortex, Fig. 1 C, the velocity is near freestream value. Analysis of the complete-cycle velocity plots near the aft portion of the wing, Fig. 1 D-G, illustrate the modest velocity gradients that occur above and through the large, convecting leading edge vortices. Vortex passage is recorded in the velocity profile as momentary but systematic deviations from near freestream values. These velocity maxima even though the vortex structures are larger, are not as pronounced as those recorded at more forward chord positions where the vortex is smaller. Analysis of velocity fluctuations for all probe positions indicates, as with all other test conditions on all wings, the greatest vortex-induced velocity variations at C = 0.17c along the chordlength.

Since greatest velocity fluctuations over an oscillation cycle occur at C = 0.17c, comparisons of flow visualization and hotwire data for the STW at S = 0.67c and K = 1.0 are made at this chord location, Fig. 3. The hotwire probe is seen in the photographs in A through J as the oscillation cycle varies in ten equal increments from ϕ = 0.0 to 0.9, respectively. The averaged velocity data and related standard deviation are plotted for two complete cycles. Instantaneous local velocities coinciding with each photograph are labeled. At the start of the pitching cycle, α = 25 degrees and ϕ = 0.0, shown in Fig. 3 A, the hotwire is located near the high velocity circumference of a forming leading edge vortex and the local velocity is more than twice freestream value. As the downward pitching continues to ϕ = 0.1, shown in B, the vortex is larger and the probe is now approaching the vortex core. A corresponding decrease in velocity at point B is observed. At point C, ϕ = 0.2, the hotwire probe is visualized inside the vortex core and a velocity less than half freestream is recorded. Point D shows the probe still inside the vortex and indicates a correspondingly low

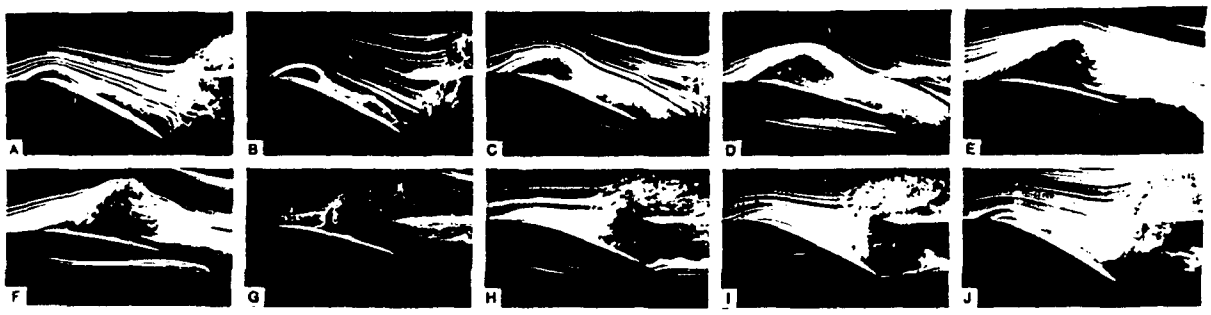

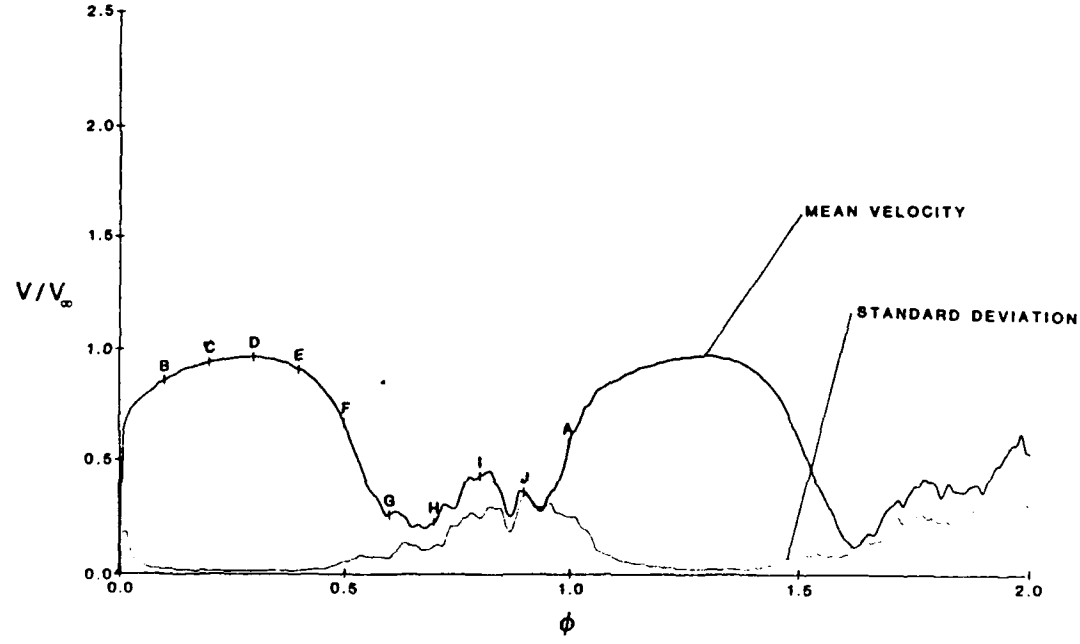

Fig. 4 Flow visualization and hotwire comparison, STW, K = 1.0, C = 1.00c, S = 1.00c.

velocity. The probe at point E is entering the higher velocity region near the forward edge of the vortex as aft convection of the vortex continues. Points F-I show a seemingly non-cohesive, turbulent vortex traversing the surface aft of the probe position. The velocity continues to increase from F to I as the potential flow reattaches to the wing surface after passage of the leading edge vortex. Point J appears to show vorticity coalescing for the initiation of a new, large scale vortex near the leading edge of the wing.

The hotwire probe location at the trailing edge of the wing reveals velocities of the dynamic stall vortex as it passes through this chord location. A flow visualization versus velocity comparison at C = 1.00c for the STW at S = 1.00c and K = 1.0 is shown in Fig. 4. The peak velocities at this chord position do not attain magnitudes as great as those shown at C = 0.17c. Passage of the leading edge vortex is recorded by decreased velocity values. During vortex initiation, growth and early convection, the probe does not encounter vortical flow and the recorded velocities are near freestream values. When the leading edge vortex is shed, Fig. 4 H, I and J, the shedding of free vorticity from the lower surface can be seen at the trailing edge.

The standard deviations of velocity fluctuations for the ten averaged data runs are also plotted for two oscillation cycles in Figs. 3 and 4. In both figures, the standard deviation increases when the probe is inside the leading edge vortical structure. This increase probably correlates with very local velocity fluctuations in the interior of the vortex. The standard deviation plots begin to increase as soon as the hot wire probe records the velocities interior to the vortex and decrease when the probe begins to sense the more structured, high speed velocities of the vortex circumference. When the probe is not encountering interior vortex flows, standard deviations are very small.

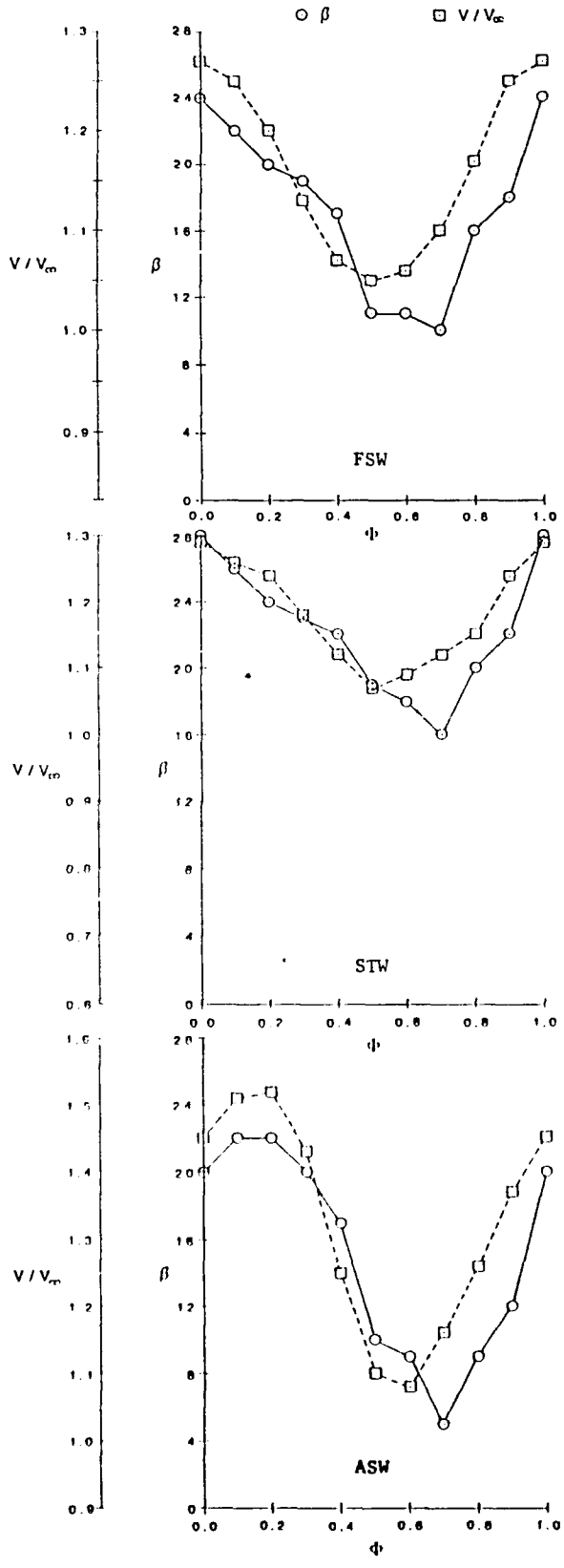

Fig. 5 Velocity and β angle comparisons, K = 1.0, C = 0.17c, S = 0.00c, FSW, STW and ASW.

The spanwise deflection angle, β, of the flow at the wingtip was recorded from top view flow visualization. Phase-dependent comparisons of these β angles with anemometric velocity measurements at the wingtip are shown in Fig. 5 A, B and C. The velocity data points were plotted for chord location C = 0.17c, however, identical velocity trends were noted at all chord locations from leading to trailing edge. The FSW data, shown in Fig. 5 A, illustrates similar trends in velocity and β measurements throughout one complete pitching cycle (Φ = 0.0 to 1.0). The high velocity and β magnitudes occur during high angle of attack portions of the pitching cycle while the minimum values are recorded near minimum α portions. This velocity profile was also observed inboard along the span until nearly midspan, S = 0.67c, where effects of leading edge vortex development altered the shape of the velocity curve. Similar comparative velocity and β angle results are noted for the STW in Fig. 5 B. Spanwise observations reveal that this wingtip velocity profile exists inboard along the span only to the S = 0.33c location. The ASW data, shown in Fig. 5 C, again, shows similar trends in velocity and β angle. These profiles display the highest magnitudes on both plots during the downstroke of the cycle after passage of maximum angle of attack. The minimums are also shifted until the upstroke of the *cycle after minimum α is passed.* The leading edge vortex effect is observed over the aft portion of the ASW even at the wingtip location. The previously observed wingtip profiles for the FSW and STW were not observed for the ASW at any span location inboard from the tip.

A spanwise visualization comparison for each wing at K = 1.0 and Φ = 0.2 is shown in Fig. 6. These photographs depict the wingtip flow dominated regions and the leading edge vortex development as the span location varies from wingtip (S = 0.0c) to far inboard (S = 1.33c). Helical wingtip vortices are seen for all three wings at the wingtip. Even when the vertical smoke sheet impinges the wings at 0.17c inboard, smoke is pulled around the wingtip from the pressure to the suction surface indicating a strong wingtip effect. Near the leading edge of the ASW at this span position, a leading edge vortex forms inboard of the wingtip flow. The FSW and STW show no indications of a leading edge vortex formation at this location. At S = 0.33c, the FSW and STW evince a shear layer across the wing surfaces with only a slight flow disturbance near the leading edge. This suggests early coalescence of vorticity into a large scale vortex. The ASW at this span location elicits a large leading edge vortex structure which covers nearly half the wing top surface. As the smoke sheet is moved inboard, S = 0.50c, a leading edge vortex and second vortical structure are visible on all three wings.

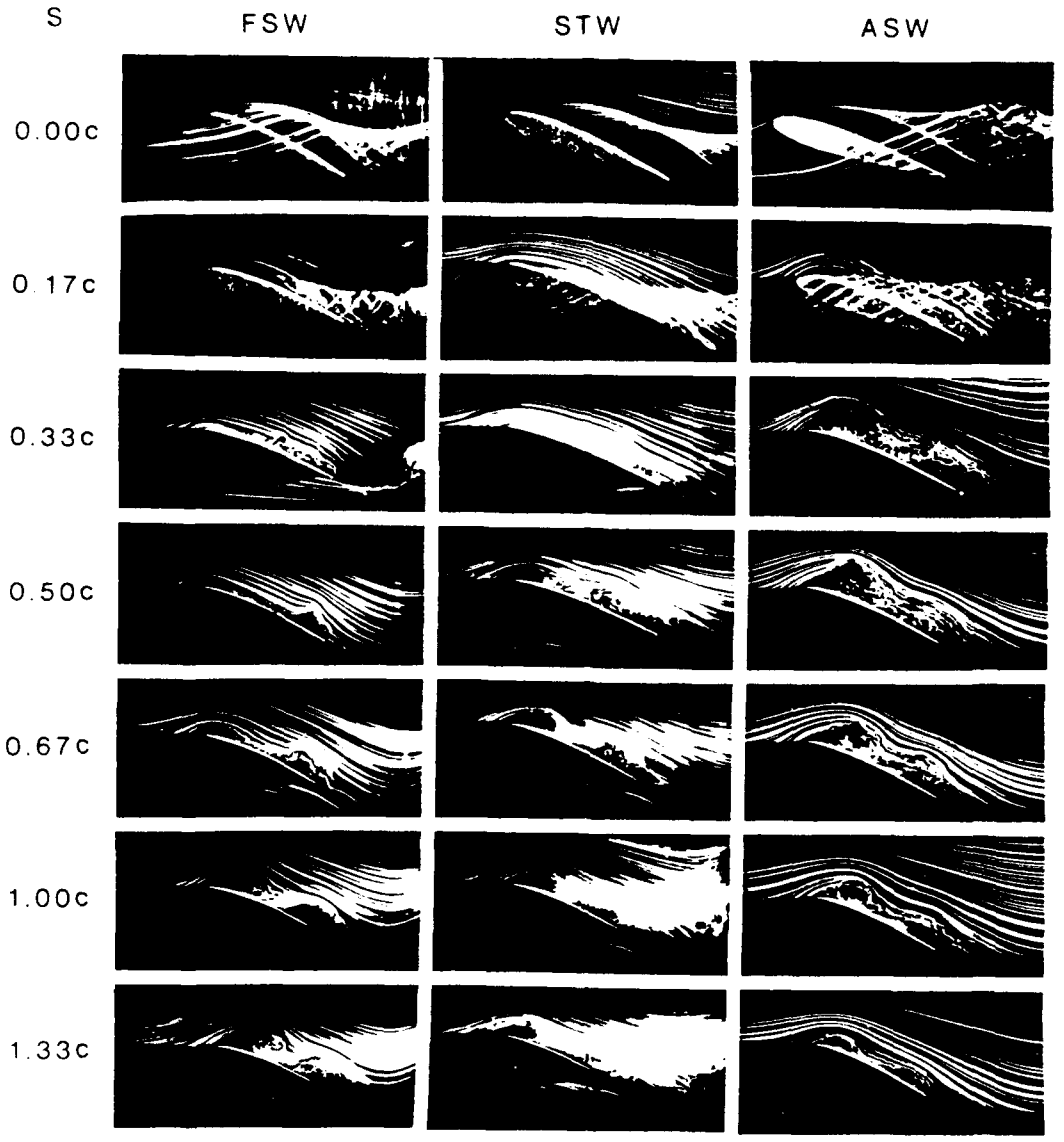

Fig. 6 Spanwise visualization comparisons, K = 1.0, ϕ = 0.2.

The size of the leading edge structure increases for the FSW, STW and ASW, respectively. Progressing further inboard, the size of the leading edge vortex on the FSW and STW increases until, at S = 1.00c, the leading edge vortices on all three wings appear similar in size. At this span location, the three-dimensional effects for each wing may reduce to nearly two-dimensional phenomenon. Further inboard, S = 1.33c, the leading edge vortex on the FSW continues to increase in size while the ASW structure decreases.

A comparison of local velocity profiles across the wingspan at C = 0.17c is shown in Fig. 7 A, B and C for the FSW, STW and ASW, respectively. The FSW and STW show very little leading edge vortex effect at the wingtip, S = 0.00c. However, the local velocity of the ASW increases at the wingtip during the pitching cycle, ϕ = 0.0 to 0.3, when a strong leading edge vortex is forming on the top surface immediately inboard of the wingtip. At S = 0.33c, the FSW local velocity profile indicates the presence of the visualized small, nearly nondiscernible leading edge vortex. The STW at this span location is visually observed to produce more cohesive leading edge structures, reflected by the velocity curves. The ASW curve at S = 0.33c graphically represents the visualized formation and convection of a leading edge vortex. For this wing, at ϕ = 0.0 to 0.6, the probe at C = 0.17c is inside the forming and developing leading edge vortex. From ϕ = 0.6 to 0.8 the leading edge structure convects aft of the probe position and the overall flow adheres to the contour of the upper wing surface near the probe. At ϕ = 0.9, a new leading

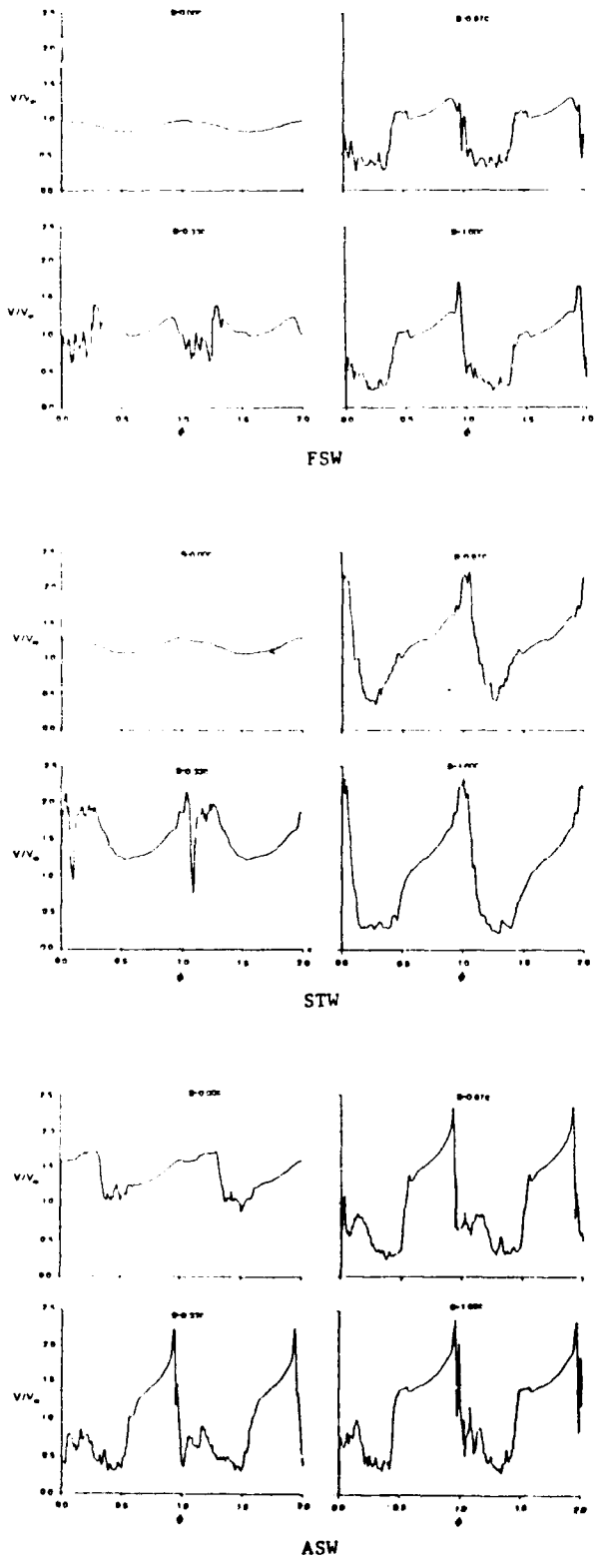

Fig. 7 Velocity profiles across span, K = 1.0, C = 0.17c, FSW, STW and ASW.

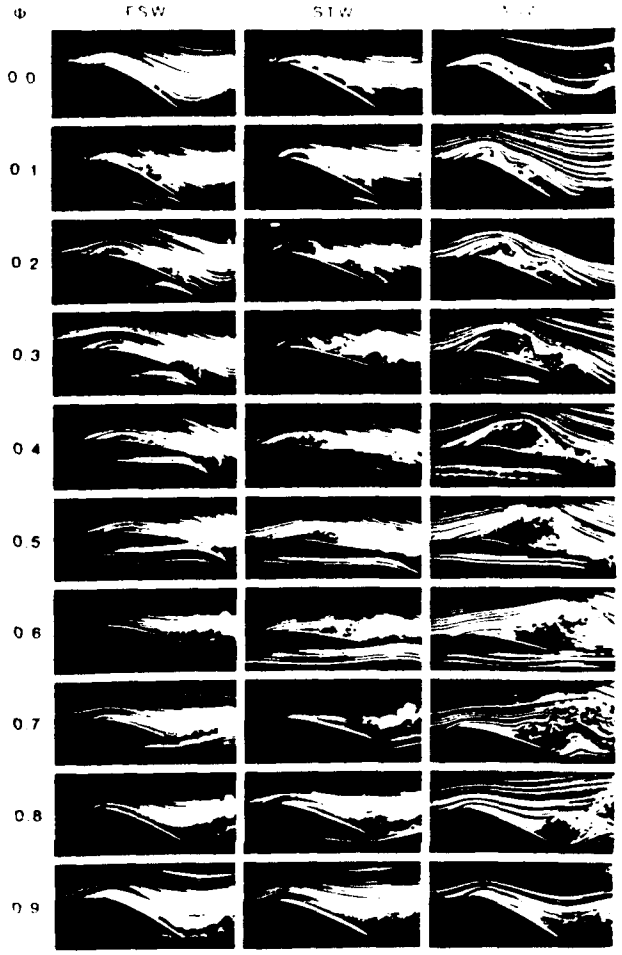

Fig. 8 Photographic comparisons over one pitching cycle, K= 1.0, S = 0.67c.

edge vortex is visualized forming and the probe is in the high velocity flow near the forward edge of this leading edge structure.

Flow visualization photographs depict more cohesive leading edge structures at S = 0.67c and S = 1.00c than near the wingtip for all three wings. This coincides with the more succinctly perturbed local velocity measurements shown for these span locations in Fig. 7 A, B and C. The overall magnitude of the FSW velocity curves is not as high as the STW or ASW. This seems to reflect the smaller size and shorter convective paths observed during flow visualization. A visualization comparison of the three wings over one complete pitching cycle at S = 0.67c is shown in Fig. 8.

Each wing geometry was tested at identical chordwise and spanwise locations for three K values, 0.6, 1.0 and 1.4. Since temporal leading edge vortex formation is K value dependent, a K value change shifted the velocity peaks to different phase points in the oscillation

cycle for all three wings. Overall velocity peak fluctuations were compared for each wing at each K value. Changes in K value produced insignificant magnitude changes in the FSW velocity profiles. The STW profiles show little fluctuation with K value change except in the span region from S = 0.67c inboard. In this region, higher K values produced larger variations in the velocity peaks. The ASW velocity profiles show greater velocity variations for smaller K values across the entire wing span.

A special note must be made in regard to velocity sampling of the three-dimensional flows. In almost all of the above velocity characterizations, the angles at which the flows intercept the hotwire probes were constant. In many cases, the incidence angles were not orthogonal to the hotwire sensor. But, the angles were consistent from one test condition to the next across most span and chord sites. Thus, although overall absolute velocities were undoubtedly less accurate than desired, comparative variations or fluctuations in local velocities were likely to be very reliable.

Discussion

Since size, strength and position of vortical structures are somewhat difficult to measure using visualization alone, hotwire anemometry was used to verify and extend the visualization results. The chordwise and spanwise hotwire investigations reveal predictable velocity distributions which correlate well with flow visualization analysis of the unsteady flow field. Previous anemometric measurements obtained by Robinson and Luttges[9] for velocity perturbations in and about leading edge vortices formed on airfoils show reliable spatial velocity fluctuations consistent with passage of the vortex. Maximum velocities were observed with the hotwire probe tangent to the vortex circumference. Probe positions localized within the vortex center or core show velocity minimums. Identical fluctuation characteristics of vortex passage signatures were observed and documented in Fig. 2. This chordwise investigation depicts high local velocities when the probe is positioned tangential to the edge of the leading edge vortex C = 0.00c. As the probe is positioned near the center of the vortex core C = 0.17c, measured velocity decreases to a minimum. At positions further aft, the velocity magnitudes recover to near freestream values. This local velocity plot verifies leading edge vortex position as well as indicates relative vortex strength at the measured positions.

The complete velocity profiles of Figs. 1, 3, 4, and 7 show very high repeatability of the velocity fluctuations. Each of the two complete oscillation cycles across ten consecutive trials show very similar velocity characteristics. These profiles confirm the occurrence of high peak velocities when the anemometer probe is nearly tangent to the vortex circumference. When the leading edge vortex center and hotwire probe position spatially coincide, minimum velocities are observed. As the leading edge vortex grows larger and convects downstream, the magnitude of the velocity peaks recorded at aft hotwire probe positions decreases. This trend is verified by observations (Robinson and Luttges[9]) and by potential and viscous flow theory (Schlichting [21]). Thus, the observed local velocity profiles graphically illustrate the time history of leading edge vortex development and convection as observed during previous flow visualization tests.

The velocity and β angle comparisons over one complete oscillation cycle, Fig. 5, illustrate flow field dynamics near the wingtip for each wing sweep test configuration. In all cases, the velocity and β angle trends are coincidental throughout the pitching cycle. The wing-geometry-dependent continuation of these wingtip velocity trends to inboard sites along the span is quite consistent. The FSW wingtip velocity trends are observed inboard as far as S = 0.67c. Flow visualizations show a viscous layer in this area which prevents the shear layer vorticity from accumulating near the leading edge into a large scale, rotational leading edge vortex. This characteristic may be due to the strong spanwise flow from wingtip to wingroot for a FSW. This span-directional flow may prevent the chordwise reverse flow of vorticity toward the leading edge. Therefore, the coalescence of small, possibly turbulent, vortices into the large scale leading edge structure apparently is disrupted.

Wingtip velocity trends were observed for the STW inboard only until S = 0.33c, and for the ASW only at the forward chord positions even at the wingtip location. The flow over the STW shows little, if any, span-directional flow perseverance inboard from the wingtip vortex dominated region, S= 0.00c to 0.33c. Flow visualizations document the formation of a small leading edge vortex at S = 0.33c but no downstream convection of this structure occurs. At phase angles approaching the minimum angle of attack, this structured leading edge vortex dissipates into a shear layer that dominates the entire STW top surface. The ASW exhibits spanwise flow from the wingroot toward the wingtip. This fluid motion resists the inboard flow produced near the wingtip by the wingtip vortex. Vorticity is accumulated into a structured leading edge vortex on the ASW surface at spanwise points proximal to the wingtip. These structures are observed by both anemometry and flow visualization.

As mentioned previously, the FSW and ASW geometries produce spanwise fluid motion along the top surface. The minimum pressure line for each wing runs roughly parallel to the wing leading edge. Since the airflow is not orthogonal to this line, some span-directional velocities are produced. This characteristic can be verified using incompressible, constant viscosity, Navier-Stokes equations of motion[21]. The spanwise flow promotes different stall characteristics for the FSW and ASW. These regional separation characteristics visualized for each wing during static tests predict spanwise areas of large scale vorticity when oscillating pitch motions are applied to the wings.

The spanwise investigations shown in Fig. 7 graphically depict sweep angle effects as well as wingtip and leading edge vortex interactions. As predicted during flow visualization studies, local velocities near the wingtip are normally lower than those recorded at more inboard locations at the same chord position. This verifies the suppression of vortex-structured vorticity near the wingtip. The fluid flow near the wingtip for the ASW quite effectively resists wingtip effects and higher local velocities are observed in this region. The complete velocity profiles over two oscillation cycles accurately show wingtip effect and leading edge vortex position and strength at any observed span location.

Changes in vortex structure and velocity strength caused by different K values are nominal when compared to wing geometry effects. The range of K values investigated, K = 0.6 to 1.4, produced predictable gradients in leading edge vortex position and strength related to pitch cycle. The velocity maxima and minima for the K = 1.4 experiments were only noticeably larger than those for other K values at chord locations of approximately midchord.

The extensive flow visualization and hotwire anemometry data together with two-dimensional flow characterizations may now be used to analyze the three-dimensional fluid dynamics about unsteady wings with varying sweep geometries. Analysis of the dynamic stall process on unsteady two-dimensional airfoils has been documented[6]. The process begins with the increasing angle of attack of the wing. During this portion of the oscillation cycle, a high-vorticity boundary layer is formed on the upper surface of the wing. This layer initiates due to viscous diffusion and the pressure gradients formed by the wing dynamics. The low-momentum, high-vorticity layer near the leading edge resists external velocities and moves forward on the wing. As the sinusoidal cycle progresses toward maximum angle of attack, the geometric α change diminishes while the effective α continues to increase. Even during the decreasing α downstroke of the cycle, the effective α remains high creating high potential flow velocities which cause the outer flow forces to overcome the inner, viscous, reverse flow resistance. In this cyclic region, the surface vorticity coalesces into a large scale dynamic stall vortex. This vortex continues to grow and disturb the potential flow as α decreases. As α decreases toward minimum, the potential flow forces the rotating vortex to traverse the wing surface toward the trailing edge. This dynamic stall process is observed for wing geometries far inboard from the wingtip effect.

The initiation and growth of a large scale vortex is isolated forward and aft of the minimum pressure point on the chord of the wing. Under most dynamic conditions, a second seemingly same rotational, large scale vortex, smaller than the leading edge structure, is formed aft of this minimum pressure location. This second vortex also traverses the wing during the downstroke of the cycle. As this aft structure sheds from the trailing edge of the wing, the leading edge vortex decreases in size and, in some dynamic cases, dissipates into a shear layer and is no longer discernible on the upper surface. This phenomenon is observed by flow visualization and documented by anemometry techniques.

The explicit roles of three-dimensional sweep geometry in vorticity formation, transport and accumulation can now be discussed further. The unsteady fluid motion elicited by the oscillating FSW illustrates more diverse flow characteristics than the other two wing geometries. The wingtip effect and natural inboard spanwise flow presumably cause the distinct vorticity localizations. The wingtip flow from pressure to suction side of the wing remained strong throughout the pitching cycle. Top view photography recorded inboard spanwise flow aft of the minimum pressure chord position as far inboard along the span as S = 1.00c. The spanwise pressure gradients which cause this flow seem responsible for preventing the traversing of the leading edge vortex through this aft chord region. Vorticity accumulation near the leading edge was suppressed at span locations proximal to the wingtip. A small, weaker (shown by anemometry) dynamic stall vortex formed near the leading edge. The size and strength of this vortex increased with inboard span location. As convection began, this leading edge structure decreased in size and dissipated into the shear layer. This leading edge dissipation and shear layer formation coincided with shedding of the midchord vortex. The potential flow above the viscous region did remain somewhat contoured to the wing upper surface and no full, cataclysmic stall was noted even at high α values. This phenomenon may

enhance lift characteristics when compared to non-pitching wings.

The flow characteristics about the unsteady STW also illustrated three-dimensional wingtip effects but not as far inboard as for the FSW. Again, the leading edge vortex size increased as distance from the wingtip increased. The dissipative effect on the leading edge vortex was noted until an inboard span location of S = 0.33c was reached. The dynamic stall vortex size decrease that coincided with midchord vortex shedding continued until S = 0.67c. At S = 1.00c, the large scale vortex increased in size when the midchord vortex was shed into the wake. Farther inboard, the transient separation phenomena behaved nearly the same as at the S = 0.67c location. The STW unsteady flow dynamics may provide greater lift enhancement advantages than those observed for the FSW.

The ASW geometry provided nearly complete spanwise sites for vorticity transport and accumulation into large scale dynamic stall vortices. The disturbance of the potential flow by the leading edge vortex was recorded even at the wingtip location. Presumably, the natural root-to-tip spanwise flow across the ASW stimulates vorticity accumulation and dynamic stall near the leading edge. The leading edge vortex continued to enlarge throughout the pitching cycle, and in some dynamic cases enveloped the entire upper surface of the wing before shedding into the wake. A decrease in dynamic stall vortex size and a shear layer effect were noted for the ASW near the wingroot. Since the wing surface area covered by the vortical structure is significantly larger for the ASW, this geometry may provide the ideal fluid dynamic characteristics for unsteady lift enhancement.

Conclusions

Both flow visualization and anemometry techniques verify the dynamic spatial and temporal differences in the unsteady flow fields produced about the three sinusoidally oscillating wings differing in sweep angles. Flow visualization techniques were used to record the leading edge vortex size, position and convective tendencies. This procedure elucidates and documents comparative sweep angle effects since flow visualization photographs for each of the three wing geometries were compared for the same dynamic, chordwise and spanwise locations. The hotwire anemometry data, although not precise because of flow angularity, provide comparative corroboration of flow visualization results. The measured local velocity fluctuations revealed and documented position, size and relative velocities of the flow field structures.

Chordwise anemometric investigations conducted over the complete pitching cycle verified the formation, development and convection of the visualized leading edge vortex structure. The largest velocity peaks always occurred at C = 0.17c where vorticity was accumulating into a very cohesive leading edge structure. As this structure enlarged and convected, rotational energy dissipated and measurements in the vortex circumference indicated reduced V/V_∞ values. Chordwise investigations, when applied at identical span locations for all three wings defined significant differences in the unsteady flow field characteristics of each wing.

The spanwise comparison of flow visualization and anemometry data shows that wing sweep angles produced major changes in vortex initiation, development and convection velocity. The different interaction regions between wingtip and leading edge vortices are dramatically resolved by comparing visualized flow with recorded anemometric data. The wingtip effect suppresses the leading edge vortex near the wingtip. This effect is more evident about the FSW than the other wing geometries. The dynamic stall characteristics of the ASW allow resistance of the wingtip effect to span positions proximal to the wingtip.

The above noted differences in wing sweep angle effects on unsteady flow structures will undoubtedly affect ultimate utilization schemes on new technology aircraft. The present work shows that unsteady flow three-dimensionality can be made to vary in different but reliable fashion. For example, wing sweep angle can reliably dictate the flow structures likely to pass over downstream aircraft control surfaces. These will be important facets to integrate into future methodologies devised for controlling unsteady flow structures use in the low speed flight regime.

Acknowledgements

This work was supported, in part, by the U.S. Air Force Office of Scientific Research, Grant F4962083K0009, Dr. James McMichael, project manager. The technical assistance of W. Bank and R. Meinzer is appreciated.

References

1. Moore, M. and Frei, D., "X-29 and Forward Swept Wing Aerodynamic Overviews," AIAA - 83-1834, AIAA Applied Aerodynamics Conference, Danvers, Massachusetts, July, 1983.

2. Uhad, G.D., Weeks, J.M. and Lange, R., "Wind Tunnel Investigation of Transonic Aerodynamic Characteristics of Forward Swept Wings," J. Aircraft, 20(3), pp. 195-202, March 1983.

3. McCroskey, W.J., "Unsteady Airfoils," Ann. Rev. Fluid Dyn. Annual Reviews, Palo Alto, California: 1982, pp. 185-211.

4. McAlister, K.W. and Carr, L.W., "Water Tunnel Visualizations of Dynamic Stall," Journal of Fluids Engineering, Vol. 1D1: pp 376-380, September 1979.

5. McCroskey, W.J., Carr, L.W. and McAlister, K.W., "Dynamic Stall Experiments on Oscillating Airfoils," AIAA - 75-125, AIAA 13th Aerospace Sciences Meeting, Pasadena, California, January 1975.

6. Reynolds, W.C., and Carr, L.W., "Review of Unsteady, Driven, Separated Flows," AIAA-85-0527, AIAA Shear Flow Control Conference, Boulder, Colorado, March, 1985.

7. Reisenthel, P.H., Nagib, H.M. and Koga, D.J., "Control of Separated Flows Using Forced Unsteadiness," AIAA-85-0556, AIAA Shear Flow Control Conference, Boulder, Colorado, March 1985.

8. Luttges, M.W., Robinson, M.C. and Kennedy, D.A., "Control of Unsteady Separated Flow Structures on Airfoils," AIAA-85-0531, AIAA Shear Flow Control Conference, Boulder, Colorado, March 1985.

9. Robinson, M.C. and Luttges, M.W., "Unsteady Separated Flow: Forced and Common Vorticity about Oscillating Airfoils," Workshop on Unsteady Separated Flows, Francis, M. and Luttges, M. (eds.), University of Colorado: 1984, pp 117-126.

10. Adler, J.N., Robinson, M.C., Luttges, M.W. and Kennedy, D.A., "Visualizing Unsteady Separated Flows," Third International Symposium on Flow Visualization, Proceedings, Vol. III, Ann Arbor, Michigan, Sept. 1983, pp. 806-811.

11. Adler, J. and Luttges, M., "Three-Dimensionality in Unsteady Flow about a Wing," AIAA - 85-0132, AIAA 23rd Aerospace Sciences Meeting, Reno, Nevada, January 1985.

12. Gad-el-Hak, M. and Ho, C., "Three-Dimensional Effects on a Pitching Lifting Surface," AIAA - 85-0041, AIAA 23rd Aerospace Sciences Meeting, Reno, Nevada, January 1985.

13. Gad-el-Hak, M.; Ho, C.; and Blackwelder, R.F., "A Visual Study of a Delta Wing in Steady and Unsteady Motion," Workshop on Unsteady Separated Flows, Francis, M. and Luttges, M. (eds.), University of Colorado: 1984, pp 45-50.

14. Carta, F.O., "Unsteady Stall Penetration of an Oscillating Swept Wing," Workshop on Unsteady Separated Flows, Francis, M. and Luttges, M. (eds.), University of Colorado: 1984, pp 28-37.

15. Ashworth, J., Waltrip, M. and Luttges, M., "Three-Dimensional Unsteady Flow Fields Elicited by a Pitching Forward Swept Wing," AIAA - 86-1104, AIAA 4th Joint Fluid Mechanics, Plasma Dynamics and Lasers Conference, Atlanta, Georgia, May 1986.

16. Gad-el-Hak, M. and Ho, C., "Unsteady Vortical Flow Around Three-Dimensional Lifting Surfaces," AIAA Journal, Vol. 24, No. 5, pp. 713-721, May 1986.

17. Ashworth, J. and Luttges, M., "Comparisons in Three-Dimensionality in the Unsteady Flows Elicited by Straight and Swept Wings," AIAA-86-2280CP, AIAA Atmospheric Flight Mechanics Conference, Williamsburg, Virginia, August 1986.

18. Freymuth, P.; Finaish, F.; and Bank, W., "Visualization of Wing Tip Vortices in Unsteady and Steady Wind," AIAA - 86-1096, AIAA 4th Joint Fluid Mechanics, Plasma Dynamics and Lasers Conference, Atlanta, Georgia, May 1986.

19. Robinson, M.C.; Gilliam, F.; Helin, H.; Russell, J. and Walker, J., "Visualization of Three-Dimensional Forced Unsteady Separated Flow." AIAA - 86-1066, AIAA 4th Joint Fluid Mechanics, Plasma Dynamics and Lasers Conference, Atlanta, Georgia, May 1986.

20. Helin, H.E., Robinson, M.C. and Luttges, M.W., "Visualization of Dynamic Stall Controlled by Large Amplitude Pitching Motions," AIAA-86-2281-CP, AIAA Atmospheric Flight Mechanics Conference, Williamsburg, Virginia, Aug. 1986.

21. Schlichting, H., Boundary-Layer Theory, McGraw-Hill Book Company, Sixth Edition, 1968, pp. 61-108.